

# Pulsed-Field-Gradient NMR with Magic-Angle Spinning:

## Diffusion Studies and NMR Microscopy of Heterogeneous Materials

**André Pampel**

Universität Leipzig, Fakultät für Physik und Geowissenschaften,  
Linnéstraße 5; D-04103 Leipzig, Germany  
Current address: Max Planck Institute for Human Cognitive and Brain  
Sciences, Stephanstraße 1a, D-04103 Leipzig, Germany

**Frank Engelke, Dieter Groß, Thomas Oerther, Klaus Zick**

Bruker Biospin GmbH, Silberstreifen, D-76287 Rheinstetten, Germany

### Introduction

High-resolution magic-angle-spinning (HR-MAS) NMR spectroscopy is a well-established tool for studying heterogeneous systems, especially semi-solid materials such as lipid membranes [1-4], drug delivery systems, cell suspensions [5,6], biopsy samples [7], molecules adsorbed in zeolites [8,9], and resin-bound molecules [10]. In such systems MAS sufficiently suppresses the otherwise disturbing anisotropic interactions such as magnetic susceptibility, chemical shift anisotropy or even dipolar coupling. At already modest rotation frequencies, well-resolved  $^1\text{H}$ -NMR spectra can be observed, and the straightforward application of NMR methods commonly used for liquid samples is possible.

In order to facilitate gradient-assisted high-resolution multi-dimensional NMR under HR-MAS conditions, the corresponding probes are generally equipped with coils for creating pulsed field gradients (PFG) [11]. Recently, it has been shown that lateral diffusion can be conveniently studied using a combination of PFG and MAS techniques [3,5,12,13], and the method has been successfully applied in the study of diffusion properties in many of the materials mentioned above. Furthermore, suppression of large solvent signals and signals of mobile components has been demonstrated using spin-echo-based diffusion filtering [14-16]. The combined use of PFG and MAS facilitates the study of the diffusion of several different molecules simultaneously.

### Strong Gradients with MAS Probes

Although HR-MAS probes provide excellent spectroscopic resolution, in the standard configuration they still lack the capability for very strong pulsed field gradients. For comparison, a conventional HR-MAS probe provides a maximum gradient of ca. 0.5 T/m (50 G/cm) along the rotor axis, while specialty probes designed for PFG-NMR can achieve ca. 30 T/m (3000 G/cm) along the z-axis. Such strong gradients are highly desirable since they allow the detection of very slow diffusion processes or diffusion within a very short time frame.

The gradient coil in an MAS probe usually consists of wires that are wound around the MAS stator. However, this design has some disadvantages: the Q factor of the resonance circuits may decrease with negative effects on rf efficiency ( $B_1$  field and detection sensitivity). In addition, the large forces result-



**Fig. 1:** Bruker components for a HR-MAS-PFG system. A conventional standard-bore HR-MAS probe (left) is inserted into a conventional XYZ gradient system (right) as used for NMR microscopy (Micro2.5, 40 mm i.d.), providing 25 mT/m (2.5 G/cm) per ampere of current.

ing from high currents in the gradient coil within the static  $B_0$  field mean that mechanical stability might become an issue at high gradient strengths.

In the following we describe a novel approach for achieving reasonably strong field gradients, namely the use of a conventional standard-bore MAS probe inserted into a microimaging gradient system [17]. The components of the system are shown in **Fig. 1**. The advantages of this scheme are as follows.

- The gradient coils are not mounted on the MAS stator and are separated from the rf components, thus minimizing any possible negative influence on the rf properties of the NMR coil.
- External water-cooling of the gradient coils allows the use of high currents to obtain high gradient strengths.
- The relatively large diameter of the gradient system results in excellent linearity of the field gradients over the NMR sample.
- No torque acts on the MAS stator during gradient pulses; mechanical stability and orientation of the rotor axis are not compromised, so that optimal NMR results are obtained.

The microimaging gradient system can generate a field gradient  $\mathbf{G}$  with three independent components

$$G_x = \partial B_z / \partial x, \quad G_y = \partial B_z / \partial y, \quad G_z = \partial B_z / \partial z \quad (1)$$

where the direction of the magnetic field  $\mathbf{B}_0$  defines the z-direction.

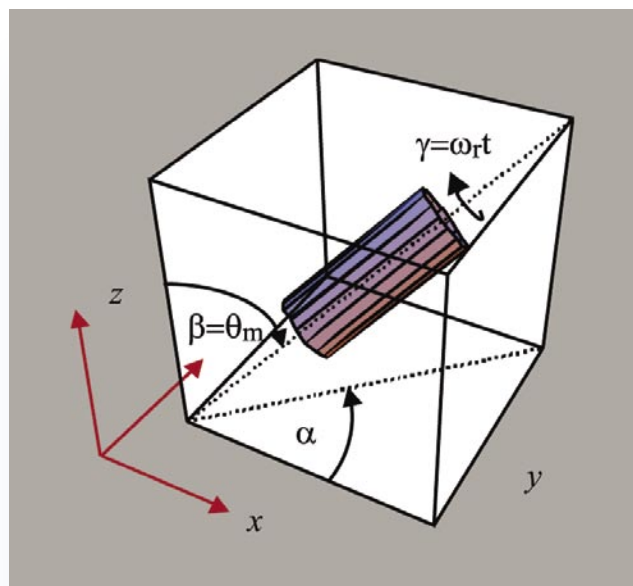


**Fig. 2:** The three Euler angles  $\alpha$ ,  $\beta$ ,  $\gamma$  describe the coordinate transformation from the MAS rotor frame to the laboratory frame.

The additional field  $\mathbf{B}$  generated by the gradients for a spin at position  $\mathbf{r} = (x, y, z)$  in the laboratory frame is given by

$$\mathbf{B} = \mathbf{G} \cdot \mathbf{r} \quad (2)$$

The position vector  $\mathbf{r}$  in the laboratory frame for a spin located at position  $\mathbf{r}_R = (x_R, y_R, z_R)$  in the rotor frame is modulated by sample spinning. The field acting on a spin located at  $\mathbf{r}_R$  can be calculated using an orthogonal transformation of  $\mathbf{r}_R$  to  $\mathbf{r}$ . This transformation is described by a set of Euler angles  $\alpha$ ,  $\beta = \theta_m$ ,  $\gamma = \omega_r t$ , as shown in **Fig. 2**, where  $\theta_m$  is the magic angle and  $\gamma$  represents the time-dependent angle of rotation about the rotor axis with angular frequency  $\omega_r$ .

If the MAS rotor axis is oriented with  $\alpha = 45^\circ$  and the field gradient  $\mathbf{G}$  in the laboratory frame has three equal components

$$G_x = G_y = G_z = G \quad (3)$$

then the gradient field in the rotor frame has the components

$$\mathbf{B}_R = (0, 0, 3^{1/2} G z_R) . \quad (4)$$

Thus, the field gradient with amplitude  $3^{1/2}G$  is oriented along the magic angle axis, and the dephasing and rephasing of magnetization during gradient pulses depends only on the coordinate  $z_R$  in the rotor frame. For our experiments the angle  $\alpha$ , the azimuthal orientation of the MAS stator, was adjusted by rotating the HR-MAS probe inside the microimaging gradient system.

## Materials and Methods

To demonstrate our setup, we chose a sample containing the monoacylglycerol 1-(9-*cis*-octadecenoyl)-*rac*-glycerol or 1-monoolein (MO) in  $D_2O$ , which forms a so-called bicontinuous cubic liquid-crystalline phase composed of a minimal surface forming a lipid bilayer that is interlaced with water channels. Because of the bilayer nature cubic phases can be considered as models for lipid membranes, and some applications with cubic phases have been reported [3, 18-20].

The diffusion properties of molecules embedded in the lipid bilayer of a cubic phase are well-suited for evaluating our HR-MAS-PFG system. The diffusion coefficient of lipids in cubic phases is on the order of  $10^{-12}$  m<sup>2</sup>/s and, as a result of the pseudo three-dimensional diffusion along curved surfaces, the spin-echo signal attenuation is purely Gaussian. Therefore, any deviation from linear behavior in the plot of the logarithm of the relative spin-echo amplitude versus the squared gradient strength would signify imperfections in the experimental setup.

Cubic phases have the advantage that the  $^1H$  spectra with MAS are well resolved. The observed linewidth was 1 - 3 Hz, and the spectra were thus highly sensitive to possible field instabilities

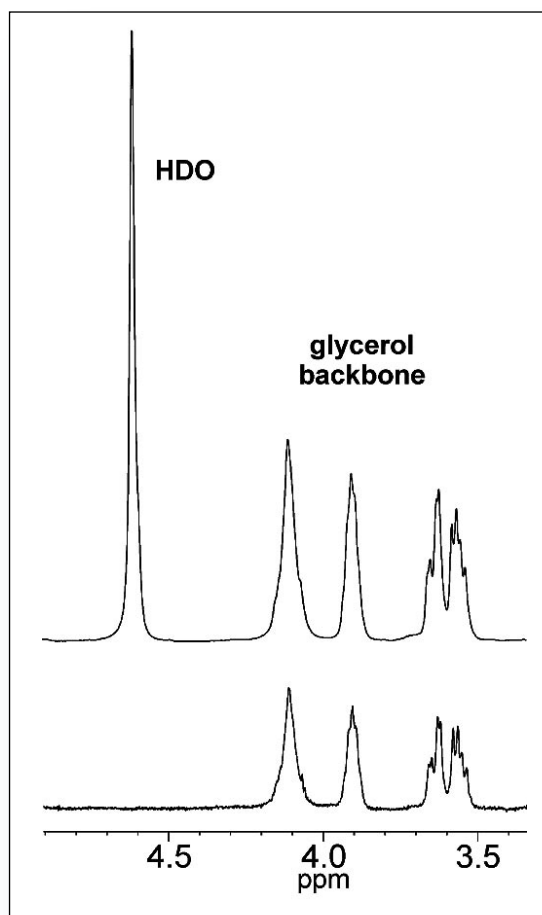


**Fig. 3:**  $^1\text{H}$  HR-MAS NMR spectra (400.13 MHz) of a cubic phase composed of 1-monolein in  $\text{D}_2\text{O}$ , recorded at 307 K and a rotation frequency of 4 kHz. The spectra show the expanded region of the glycerol backbone. The upper spectrum was measured with a pulse-acquire sequence. The lower spectrum (increased vertical scale) was measured with a stimulated-echo PFG sequence at the maximum gradient strength available. Diffusion weighting resulted in disappearance of the HDO signal from rapidly diffusing water. Note that the lineshape for the glycerol signals is essentially the same with or without PFG.

that might be caused by strong gradients with long pulse durations (eddy current effects, mechanical instabilities, etc.).

The experiments were performed on an Avance 400 wide-bore spectrometer equipped with three GREAT 60 gradient current power supplies and a standard-bore  $^1\text{H}/^{13}\text{C}$  HR-MAS probe inserted into the Micro2.5 gradient system so that the sample was centered in the isocenter of the gradient system. The standard XWIN-NMR 3.5 and ParaVision 2.0 software packages were used.

Diffusion studies were performed using a modified stimulated-echo (STE) PFG sequence which employed for diffusion weighting two PFG pulse sandwiches, each consisting of bipolar (+/-) 1-ms sine-shaped gradient pulses separated by a  $180^\circ$  rf pulse. The delay  $\Delta$  between bipolar sandwiches was 200 ms. The maximum magic-angle gradient strength available was 2.6 T/m at 60 A current in the X, Y, and Z coils.

**Fig. 3** compares spectra obtained with either a pulse-acquire sequence or the STE-PFG sequence. No influence of gradient pulses on signal lineshape or position was observed, even at the highest available gradient strength.

The semi-logarithmic plot of the spin-echo attenuation  $\psi$  for lipid signals vs. the squared gradient strength is shown in **Fig. 4**. There is no significant deviation from linear behavior. The diffusion coefficient obtained is in good agreement with those recently published.

The hardware configuration described above can be used to investigate other systems such as cells, tissues, zeolites, etc. Thus, it is possible to study diffusion in systems that, up to now, were not readily accessible with PFG NMR in combination with high-resolution spectroscopy [21].

## NMR Microimaging of Rotating Samples

The combination of MAS with the spatial localization methods used in MRI offers the possibility of a tremendous reduction in signal linewidths together with the ability to obtain spatially resolved images or spectra from localized volumes of semi-solid samples. Such experiments were initially developed by some pioneers who built dedicated hardware and created dedicated acquisition methods [22-26]. Here, we demonstrate the use of the hardware described above without modification, thus profiting from the advantages already discussed.

The most direct way to record three-dimensional images of the spin-density  $\rho(x_R, y_R, z_R)$  within an MAS rotor requires orientation of the effective gradients along the rotor's axes and synchronous "co-rotation" of the gradient components ( $G_x, G_y, G_z$ ) with the rotation of the sample. The generation of the  $z_R$ -gradient has been described above (Fig. 2). In order to obtain the required  $x_R$ - and  $y_R$ -gradients for imaging, the effect of gradients applied in the laboratory frame on spins

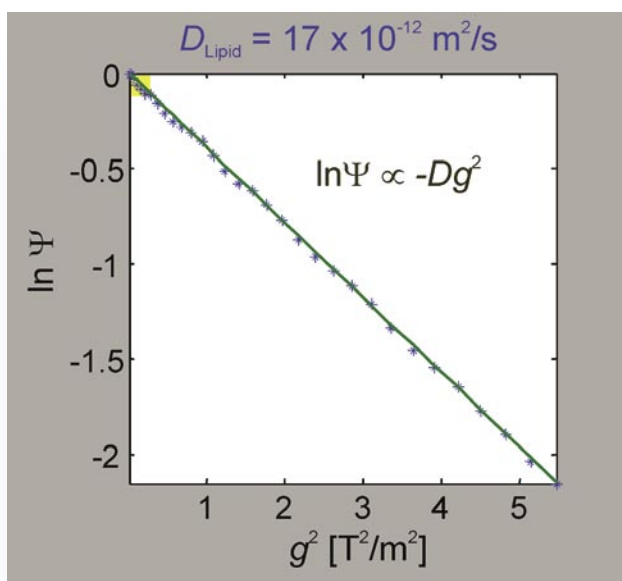


**Fig. 4:** Plot of the logarithm of the spin-echo attenuation of the lipid signals  $\psi$  vs. the gradient strength squared. The solid line is the linear least-squares fit. The yellow rectangle (upper left) marks the region of gradient strengths accessible with a standard HR-MAS probe with internal gradient coil.

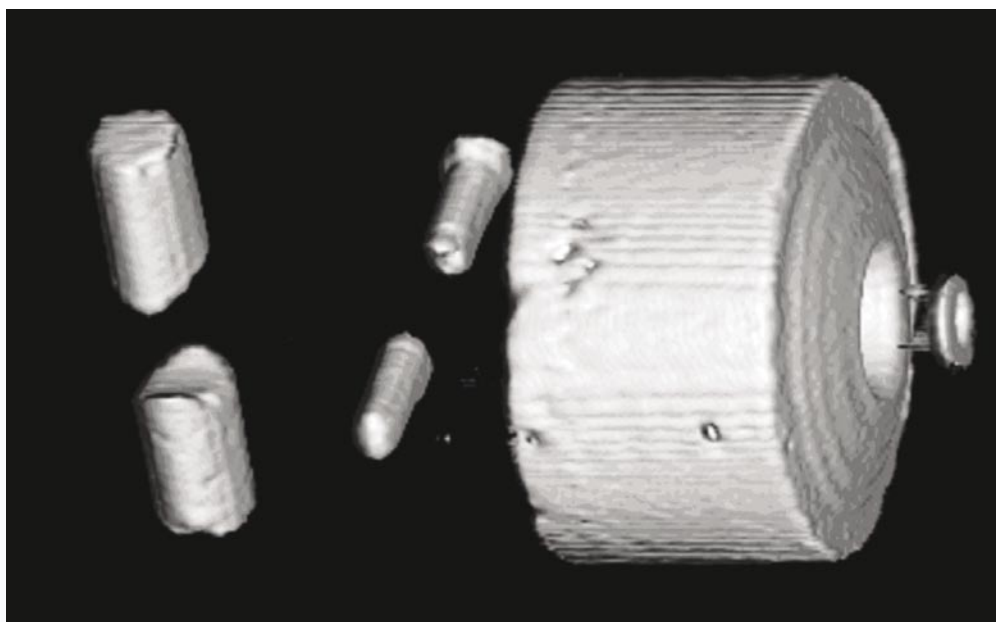


**Fig. 5:** 400 MHz  $^1\text{H}$  image of water in a Kel-F phantom rotating at 3500 Hz in a HR-MAS probe. The large cylindrical form represents water centrifuged out to the rotor wall in the space left between the Kel-F cylinder and the teflon plug. Some water was also centrifuged into the outer regions of two small cylindrical holes bored into the Kel-F cylinder, perpendicular to the rotation axis. A 3D gradient-echo imaging sequence was used with synchronously rotating field gradients generated with the Micro2.5 gradient system. (Matrix size:  $128 \times 128 \times 128$ ; voxel dimensions:  $87.5 \times 35 \times 35 \mu\text{m}$ ; measurement time: 55 min) The image was rendered using the software ImageJ [27] in combination with volumeJ [28].

located in the rotor frame needs to be calculated. It is found that the simultaneous application of three sinusoidal oscillating gradients will generate a gradient of constant amplitude that follows the rotation of  $x_R$  in the rotor frame. Thus, an  $x_R$ -gradient of strength  $G$  in the rotor frame can be generated when the gradients produced by the microimaging XYZ gradient system have the following form.

$$G_x = G [ \cos(\omega_r t) / 6^{1/2} - \sin(\omega_r t) / 2^{1/2} ] \quad (5)$$

$$G_y = G [ \cos(\omega_r t) / 6^{1/2} + \sin(\omega_r t) / 2^{1/2} ] \quad (6)$$

$$G_z = -G [ (2/3)^{1/2} \cos(\omega_r t) ] \quad (7)$$

Similar expressions apply for the  $y_R$ -gradient.

The oscillating form of the gradients must be approximated by stepwise changes of the gradient strengths (digital waveform). The shortest time step used in our experiments was  $10 \mu\text{s}$ . Because of the resistance of the gradient coils and the limited bandwidth of the gradient amplifiers, the maximum current switching speed is limited. As a result, the actual current applied to the gradient coils follows a smooth curve which closely matches the theoretical form. This is also true for higher rotation frequencies, whereby an increasing speed of oscillation leads to a reduction of the maximum current passing through the coils. Nevertheless, the currents and gradients achievable at high rotation frequencies are still sufficient to generate images.

To test the accuracy of rotation-triggered MAS images, a phantom was constructed from a Kel-F cylinder (diameter 3 mm) in which three interconnected and perpendicularly arranged cylindrical boreholes were drilled with diameters of 1, 0.7, and 0.3 mm. This phantom sample was inserted into a 4-mm MAS rotor. The cylinder oriented along the spinning axis was filled

with water doped with  $\text{CuSO}_4$  (1 g/L). The rotor was tightly closed by a Teflon plug and spun at 3500 Hz.

The image obtained using a 3D gradient-echo sequence is shown in **Fig. 5**. There are no blurring effects visible, demonstrating that sample spinning is stable and that sample spinning and gradient rotation are correctly synchronized. In fact, one would not expect a better image with a stationary sample.

The performance of this MAS imaging method for solid samples was tested with a phantom constructed from the plastic insulation of an electric cable, sliced open on one side, with the inner copper wire removed and the resulting empty space filled with adamantane. **Fig. 6** shows a transverse slice (cross-section) taken from the 3D data set.

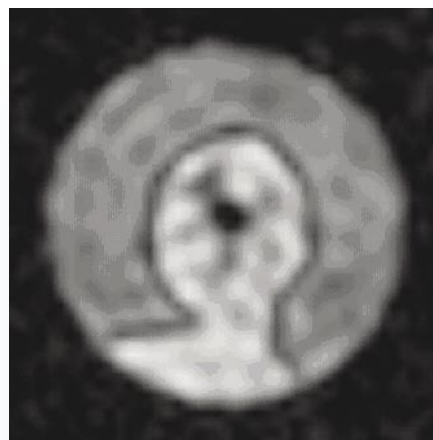


**Fig. 6:** 400 MHz  $^1\text{H}$  MAS imaging of a solid sample spinning at 5000 Hz. A single  $625\text{-}\mu\text{m}$  slice transverse to the MAS axis is displayed from the rotation-triggered 3D data set acquired from a phantom consisting of a piece of electric cable insulation (dark grey) filled with adamantane (light grey) after removal of the copper wire. The dark spot in the center is the void created by centrifugal force during sample spinning. (FOV:  $20 \times 5 \times 5 \text{ mm}$ ; matrix size:  $32 \times 32 \times 32$ ; voxel dimensions:  $156 \times 156 \times 625 \mu\text{m}$ ; measurement time: 68 min).

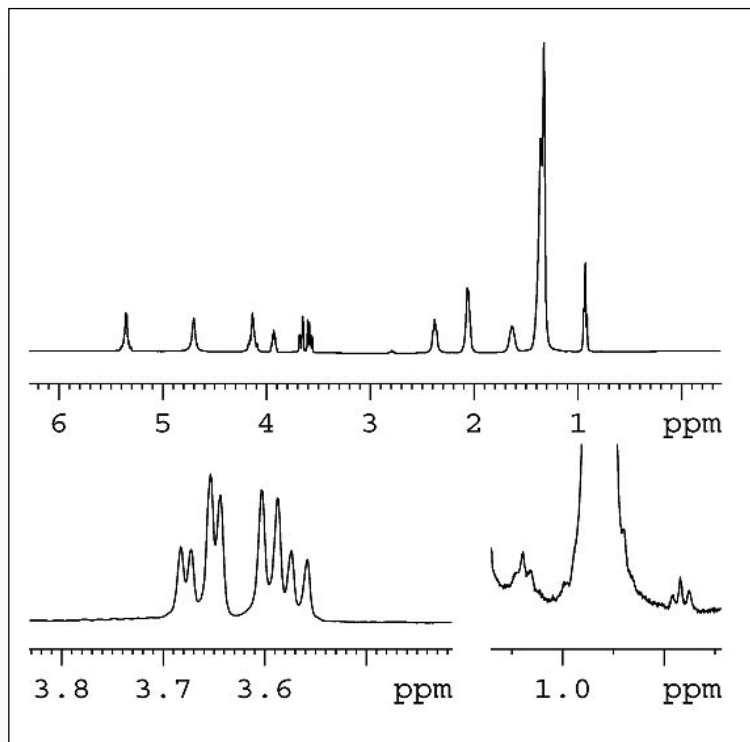


**Fig. 7:** Localized 400 MHz HR-MAS  $^1\text{H}$ -NMR spectrum of 1-monoolein in  $\text{D}_2\text{O}$  (cubic phase) from a  $300\text{-}\mu\text{m}$  transverse slice perpendicular to the rotor axis (5 kHz spinning rate, 1 transient per slice, 32 slices in 5 min).

## Localized spectroscopy of rotating samples

Spatially localized HR-MAS NMR spectroscopy was performed using the 1-monoolein sample described above. **Fig. 7** shows the  $^1\text{H}$  spectrum obtained from a  $300\text{-}\mu\text{m}$  transverse slice with the slice-selection gradient oriented along the MAS axis (effective volume ca.  $2.1\ \mu\text{L}$ ). The spectral resolution obtained was better than that observed for nonlocalized spectra of the entire rotor volume, as seen by comparing the expansion around 3.6 ppm with the spectrum in Fig. 3. The expansion around 1 ppm illustrates that for the terminal methyl group of the oleic acid moiety even the  $^{13}\text{C}$  satellites can be detected.

## Conclusion

The feasibility study presented here demonstrates that the combination of a standard HR-MAS probe with a separate three-axis gradient system designed for microimaging represents a promising alternative for typical MAS applications with semi-solid samples. With spinning samples high-quality localized  $^1\text{H}$  spectra can be obtained, and imaging or studies of molecular diffusion can be readily performed.

## References

- [1] Volke F, Pampel A. Membrane hydration and structure on a subnanometer scale as seen by high resolution solid state nuclear magnetic resonance: POPC and POPC/CI2EO4 model membranes. *Biophys J* 68 (1995) 1960-1965.
- [2] Pampel A, Strandberg E, Lindblom G, Volke F. High-resolution NMR on cubic lyotropic liquid crystalline phases. *Chem Phys Lett* 287 (1998) 468-474.
- [3] Pampel A, Reszka R, Michel D. Pulsed field gradient MAS NMR studies of the mobility of carboplatin in cubic liquid crystalline phases. *Chem Phys Lett* 357 (2002) 131-136.
- [4] Gawrisch K, Eldho NV, Polozov IV. Novel NMR tools to study structure and dynamics of biomembranes. *Chem Phys Lipids* 116 (2002) 135-151.
- [5] Chen JH, Enloe BM, Weybright P, Campbell N, Dorfman D, Fletcher CD, Cory DG, Singer S. Biochemical correlates of thiazolidinedione-induced adipocyte differentiation by high-resolution magic angle spinning NMR Spectroscopy. *Magn Reson Med* 48 (2002) 602-610.
- [6] Weybright P, Millis K, Campbell N, Cory DG, Singer S. Gradient, high-resolution, magic angle spinning  $^1\text{H}$  nuclear magnetic resonance spectroscopy of intact cells. *Magn Reson Med* 39 (1998) 337-345.
- [7] Tate AR, Foxall PJD, Holmes E, Moka D, Spraul M, Nicholson JK, Lindon JC. Distinction between normal and renal cell carcinoma kidney cortical biopsy samples using pattern recognition of  $^1\text{H}$ -1 magic angle spinning (MAS) NMR spectra. *NMR Biomed* 13 (2000) 64-71.
- [8] Pampel A, Fernandez M, Freude D, Kärger J. New options for measuring molecular diffusion in zeolites by MAS PFG NMR. *Chem Phys Lett* 407 (2005) 53-57.
- [9] Roland J, Michel D. High-resolution  $^1\text{H}$  NMR spectroscopy of adsorbed molecules in the presence of strong magnetic fields. *Magn Reson Chem* 38 (2000) 587-595.
- [10] Schröder H. High resolution magic angle spinning NMR for analyzing small molecules attached to solid support. *Combinatorial Chemistry & High Throughput Screening* 6 (2003) 741-753.
- [11] Maas WE, Bielecki A, Zilio M, Laukien FH, Cory DG. Magnetic field gradients in solid state magic angle spinning NMR. *J Magn Reson* 141 (1999) 29-33.
- [12] Pampel A, Kärger J, Michel D. Lateral diffusion of a transmembrane peptide in lipid bilayers studied by pulsed field gradient NMR in combination with magic angle sample spinning. *Chem Phys Lett* 379 (2003) 555-561.
- [13] Gaede HC, Gawrisch K. Multi-dimensional pulsed field gradient magic angle spinning NMR experiments on membranes. *Magn Reson Chem* 42 (2004) 115-122.
- [14] Rousselot-Pailley P, Maux D, Wieruszski JM, Aubagnac JL, Martinez J, Lippens G. Impurity detection in solid-phase organic chemistry: Scope and limits of HR MAS NMR. *Tetrahedron* 56 (2000) 5163-5167.
- [15] Viel S, Ziarelli F, Caldarelli S. Enhanced diffusion-edited NMR spectroscopy of mixtures using chromatographic stationary phases. *Proc Natl Acad Sci USA* 100 (2003) 9696-9698.
- [16] Chin JA, Chen A, Shapiro MJ. SPEEDY: spin-echo enhanced diffusion filtered spectroscopy. A new tool for high resolution MAS NMR. *J Comb Chem* (2000) 293-296.
- [17] Pampel A, Zick K, Glauner H, Engelke F. Studying lateral diffusion in lipid bilayers by combining a magic angle spinning NMR probe with a micro-imaging gradient system. *J Am Chem Soc* 126 (2004) 9534-9535.
- [18] Rilfors L, Khan A, Brentel I, Wieslander A, Lindblom G. Cubic liquid crystalline phase with phosphatidylethanolamine from *Bacillus megaterium* containing branched acyl chains. *FEBS Lett* 149 (1982) 293-298.
- [19] Rummel G, Hardmeyer A, Widmer C, Chiu LM, Nollert P, Locher KP, Reduzzi I, Landau EM, Rosenbusch JP. Lipidic cubic phases: new matrices for the three-dimensional crystallization of membrane proteins. *J Struct Biol* 121 (1998) 82-91.
- [20] von Eckardstein K, Patt S, Kratzel C, Kiwit JCW, Reszka R. Local chemotherapy of F98 rat glioblastoma with paclitaxel and carboplatin embedded in liquid crystalline cubic phases. *J Neuro-Oncology* 72 (2005) 209-215.
- [21] Pampel A, Engelke F, Galvosas P, Krause B, Stallmach F, Michel D, Kärger J. Selective multi-component diffusion measurement in zeolites by pulsed field gradient NMR. *Micro Meso Mat* 90 (2006) 271-277.
- [22] Schauss G, Blümich B, Spiess HW. Conditions for generating rotating gradients in MAS NMR imaging. *J Magn Reson* 95 (1991) 437-441.
- [23] Sun Y, Xiong J, Lock H, Buszko ML, Haase JA, Maciel GE. Solid-State  $^1\text{H}$  CRAMPS NMR imaging with pulsed rotating gradients. *J Magn Reson Ser A* 110 (1994) 1-6.
- [24] Buszko M, Maciel GE. Magnetic-Field-Gradient-Coil system for solid-state MAS and CRAMPS NMR imaging. *J Magn Reson Ser A* 107 (1994) 151-157.
- [25] Cory DG, Reichwein AM, Vanos JWM, Veeman WS. NMR images of rigid solids. *Chem Phys Lett* 143 (1988) 467-470.
- [26] Cory DG, Vanos JWM, Veeman WS. NMR images of rotating solids. *Chem Phys Lett* 76 (1988) 543-547.
- [27] Rasband WS. ImageJ, U. S. National Institutes of Health, Bethesda, Maryland, USA, <http://rsb.info.nih.gov/ij/>, 1997-2006.
- [28] Abramoff MD, Viergever MA. Computation and visualization of three dimensional motion in the orbit. *IEEE Trans Med Imag* 21 (2002) 296-304.